Experimental Investigation of a Shock-Accelerated Liquid Layer with Imaging and Pressure Measurement

P. Meekunnasombat, J.G. Oakley,
M.H. Anderson, R. Bonazza

November 2002

UWFDM-1215

Presented at the 15th ANS Topical Meeting on the Technology of Fusion Energy, 17-21 November 2002, Washington, DC; published in *Fusion Science and Technology* 44, 351 (2003).

FUSION TECHNOLOGY INSTITUTE

UNIVERSITY OF WISCONSIN

MADISON WISCONSIN

Experimental Investigation of a Shock-Accelerated Liquid Layer with Imaging and Pressure Measurement

P. Meekunnasombat, J.G. Oakley,
M.H. Anderson, R. Bonazza

Fusion Technology Institute
University of Wisconsin
1500 Engineering Drive
Madison, WI 53706

http://fti.neep.wisc.edu

November 2002

UWFDM-1215

Presented at the 15th ANS Topical Meeting on the Technology of Fusion Energy, 17-21 November 2002, Washington, DC; published in *Fusion Science and Technology* 44, 351 (2003).

EXPERIMENTAL INVESTIGATION OF A SHOCK-ACCELERATED LIQUID LAYER WITH IMAGING AND PRESSURE MEASUREMENT

P. MEEKUNNASOMBAT, J. G. OAKLEY,
M. H. ANDERSON† AND R. BONAZZA
Fusion Technology Institute, University of Wisconsin - Madison
1500 Engineering Dr., Madison, Wisconsin, 53706

Many inertial fusion energy reactor designs incorporate the use of liquid wall protection of cooling tubes to mitigate damage due to energetic particles and to absorb target debris. However, the pressure loading of the reactor first wall from the impulsive loading from the shock-accelerated liquid layer may be a concern. A vertical shock tube is used to conduct shock-accelerated liquid layer experiments to simulate this scenario. A shock wave contacts and accelerates a water layer down the shock tube where it is imaged in the test section. The pressure histories at various positions along the length of the shock tube are digitally recorded as well as the shadowgraph image of the breakup of the water layer. It is found that the speed of the transmitted shock wave is reduced after passing through the liquid layer; however, the pressure load at the end-wall of the shock tube is significantly increased due to the presence of the liquid layer. Water layers of two different thicknesses are studied at several Mach numbers ranging from 1.34 to 3.20.

I. INTRODUCTION

An inertial fusion energy (IFE) reaction produces a shock wave that emanates from the center of the reactor chamber to the first wall of cooling tubes. One proposed idea is to use a liquid sheet/jet of molten salt to protect the first wall from fusion debris and absorb thermal energy. The HYLIFE-II IFE reactor[1] uses a thick layer of molten salt, FLiBe[2, 3], as a liquid blanket material to protect the first wall from the fuel microexplosions that occur at frequencies of 4-10 times per second. Motions and instabilities of the liquid sheets/jets must be understood as well as the wall pressure loads from the accelerated liquid layer. Water has been widely used to study the dynamics of the molten salt experimentally[4, 5, 6]. Water mitigation of shock waves has also been studied for military safety purposes[7, 8]. However, the conditions of these experiments differ from the IFE applications since the protective liquid has not been accelerated by such explosion to the wall as in most IFE reactor designs. Impulse loads to a target from interaction between the liquid layer and a chemical detonation-generated shock have been studied[9] in an open environment chamber.

In a thick-liquid protection reactor design, the fusion target is mostly enclosed by liquid layers in all directions[10], and understanding how the shock-accelerated liquid layer generates a pressure load to the first wall in a confined environment is necessary. In this work, a large vertical shock tube is used to experimentally investigate a stationary flat liquid layer subjected to a planar shock wave acceleration in a closed system. Shadowgraph imaging of the shocked liquid layer is conducted to observe the breakup. Pressure transducers are installed along the length of the shock tube to measure the pressure histories inside the tube. Since the end-wall pressure load caused by the shocked liquid layer is expected to be nonuniform, eight pressure transducers are distributed at the end-wall of the shock tube to measure the head-on pressure load of the shock wave and the shocked liquid layer.

II. EXPERIMENTAL DESCRIPTION

Experiments are conducted in a 9.2 m long vertical shock tube with a square internal cross-section (25.4 cm sides) as shown in Fig. 1A. The driven section is filled with argon at atmospheric pressure and the water layer is located in the interface section 103.8 cm above the bottom of the shock tube and 45.9 cm above the cen-

†E-mail: manderson@engr.wisc.edu

terline of the test section window. Piezoelectric pressure transducers are flush-mounted along the inside wall (PT1-7 in Fig. 1A) and the end-wall (PTB) of the shock tube to measure dynamic pressures inside the tube at a sampling frequency of 3.6 MHz. Pressure histories along the inside of the shock tube are shown in Fig. 2 where the planar shock wave moves from the diaphragm on the left, passes the interface and the test section to the end-wall on the right at time zero. The flat water layer is supported in a square frame with a 0.94 μm thick mylar film and 19 nylon wires (0.3 mm diameter) spanning the width of the frame beneath the film to minimize sag. Preliminary experiments without water were conducted to study the effect of the support materials to the end-wall pressure history. No difference in the end-wall pressure traces was observed between experiments with the support materials and experiments without. The driven section is evacuated and filled to atmospheric pressure with argon (twice) to achieve a gas purity greater than 99%. The frame containing the water layer is then placed in the shock tube interface section. Two thicknesses of water layers are studied (6.4 mm and 12.8 mm) at several different Mach numbers ranging from 1.34 to 3.20. Effects of the initial shape of the water layer on the pressure histories at the end-wall are studied by varying the configuration of the mylar film and the support wires.

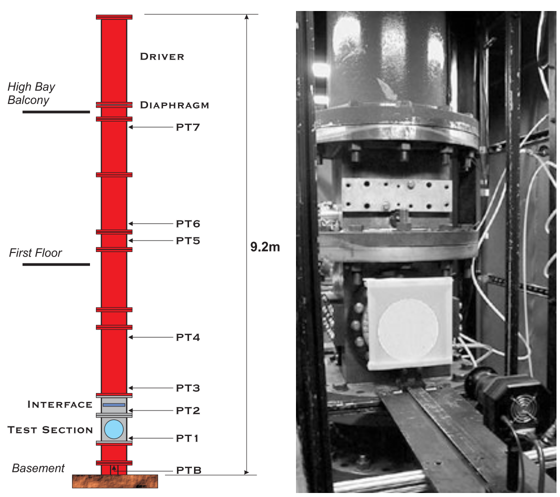

(A) (B)

Fig. 1: (A) Schematic of the shock tube and pressure transducer locations, (B) Shadowgraph optic setup on the shock tube.

The shadowgraphy technique[11] is used to image the shocked water layer at the test section. A 10 ns Nd:YAG laser pulse at a wavelength of 532 nm is used as a light source and the water layer is imaged with a 1024×1024 pixel array CCD camera. The laser beam is expanded to the diameter of the test section windows

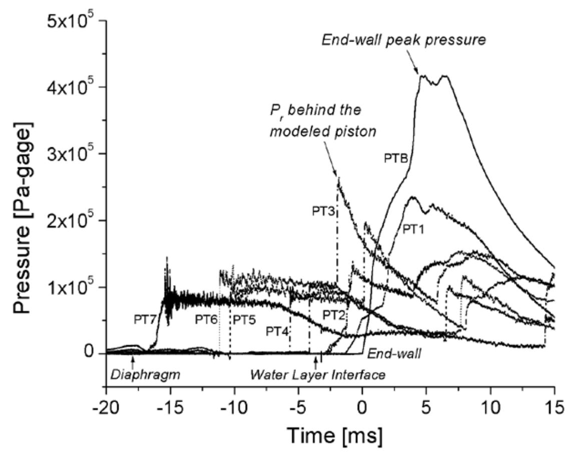

Fig. 2: Pressure histories at different locations along the length of the shock tube ($M = 1.34$, 6.4 mm of water on single layer film with wire support).

(22 cm), collimated, and then steered through the test section onto a screen that the CCD camera is focused on. Figure 1B shows a picture of the camera and screen setup at the test section.

III. THEORETICAL MODEL

The shock-accelerated water layer can be modeled as a solid piston (density ρ, thickness δ) accelerated by a high pressure reservoir P_r into a closed volume at lower pressure. Figure 3 illustrates the accelerated-piston model. P_0 is the initial pressure of the enclosed volume below the piston and this pressure increases as the piston moves down in the x direction, while the pressure behind the piston, P_r, remains constant. The initial height of the control volume, L, is the distance from the initial position of the water sheet to the end-wall of the shock tube. The process begins when the fixed piston is released and starts moving from position $x = 0$ due to $P_r > P_0$. Pressure in the compressed control volume, $P(x)$, increases from P_0 as the piston moves downwards. $P(x)$ reaches a maximum value at the time when the piston has traveled the maximum distance, or when $L - x$ is minimum. When the piston has reached its maximum displacement, the pressure in the control volume is greater than the reservoir pressure due to the compressibility of the gas and inertia of the piston. This pressure difference will result in an upwards motion of the piston and, over time, results in a reciprocating motion of the water layer. Assumptions that are made in this model are:

- The liquid layer behaves like a frictionless solid piston *i.e.*, the liquid layer does not break up
- No gas leaves the control volume
- P_r = constant
- The process is isentropic

- There are no dissipative processes.

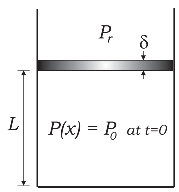

Fig. 3: Schematic of the analytical model problem.

The derivation begins with Newton's second law applied to the water layer piston,

$$P_r - P(x) = \rho\delta \frac{d^2x}{dt^2}. \tag{1}$$

Applying the isentropic assumption yields,

$$P(x) = P_0 \left(\frac{L}{L-x}\right)^{\gamma} \tag{2}$$

where γ is the specific heat ratio of the gas in the control volume ($\gamma = 1.67$ for argon). Substitution of Eq. (2) into Eq. (1) provides a second order differential equation for the motion of the piston as a function of time,

$$\frac{d^2x}{dt^2} = \frac{1}{\rho\delta}\left[P_r - P_0\left(\frac{L}{L-x}\right)^{\gamma}\right]. \tag{3}$$

Initial conditions for this equation are $x(0) = x'(0) = 0$. Equation (3) is solved numerically for x as a function of time. The maximum distance x the piston travels results in a maximum $P(x)$ which is calculated using Eq. (2).

Figure 4 shows the motion of the piston from the solution of Eq. (3). The piston is a water layer ($\rho = 1000$ kg/m^3) with a thickness $\delta = 6.4$ mm located a distance $L = 1.038$ m above the end-wall of the shock tube. P_0 is atmospheric pressure and P_r is 0.26 MPa which is the experimentally measured pressure of the gas just above the shocked water layer for an $M = 1.34$ shock wave (PT3 in Fig. 2). The maximum pressure, $P(x) = 0.608$ MPa-gage, occurs at the maximum piston travel (minimum compressed volume) and is shown in Fig. 5.

This analysis provides an upper bound for the peak pressure at the end-wall of the shock tube. In reality, there will be dissipation effects, and more importantly, the liquid layer will break up and the gas below the accelerated liquid layer will not be confined, the result being an anisentropic process with a reduction in the actual pressure load at the end-wall.

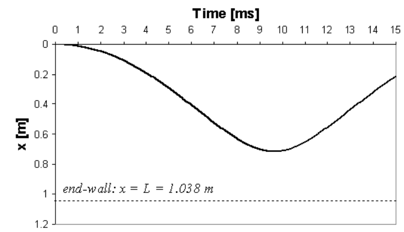

Fig. 4: Solution to Eq. (3) when the piston simulates a 6.4 mm thick water layer accelerated by an $M = 1.34$ shock wave.

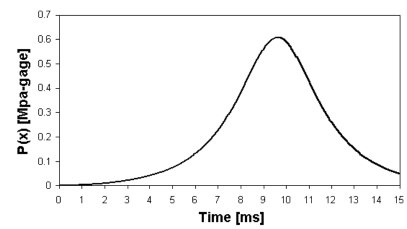

Fig. 5: Solution to Eq. (2) resulted from Fig. 4.

IV. RESULTS AND DISCUSSIONS

Figure 6A is a shadowgraph image of a transmitted shock wave and an initially flat 6.4 mm thick water layer 1.32 ms after being accelerated by a $M = 2.68$ planar shock wave. The transmitted shock wave is slightly distorted due to small nonuniformities of the initial shape of the water layer caused by the support wires. The transmitted shock wave becomes more as distorted as the sag in the water layer increases. Figure 6B is a shadowgraph image of the water layer from a separate test with the same configuration but the picture is taken 0.15 ms later than Fig. 6A. Breakup of the water layer can be clearly observed to increase between the images shown in Fig. 6A and Fig. 6B.

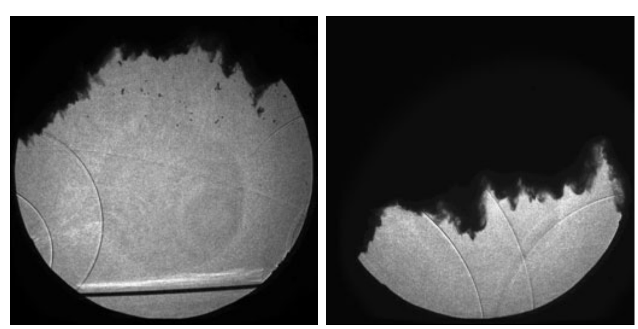

(A) (B)

Fig. 6: Shadowgraph images of the water interface. (A) 1.32 ms after being accelerated by a $M = 2.68$ shock wave, and (B) 1.47 ms after shock acceleration.

Figure 7 shows pressure traces at the end wall from experiments at $M = 1.38$. With the water layer in the interface section, the pressure rises more gradually compared to the experiment without the water layer. Slightly higher peak pressures are observed with the presence of a water layer and this is more pronounced in the experiment with the thicker water layer. Pressure histories from experiments at $M = 2.89$ change more dramatically when the water layer is present, as seen in Fig. 8. For these experiments with a water layer subjected to a strong shock wave, the pressure at the end wall rises in two steps; the first step caused by the transmitted shock wave through the water layer, and the second step, which increases pressure to the highest pressure peak, caused by the shock-accelerated water layer. The peak pressure increases significantly with the presence of the water layer–up to seven times that of the same shock strength without water.

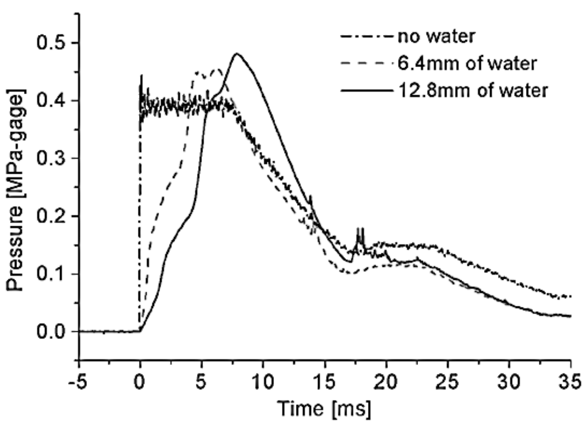

Fig. 7: End-wall pressure traces at $M = 1.38$.

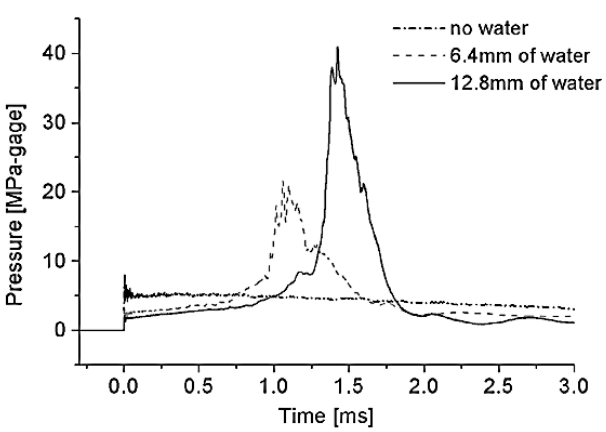

Fig. 8: End-wall pressure traces at $M = 2.89$.

End-wall pressure traces resulting from different initial water layer shapes are studied at $M = 2.65$. The support materials of the water layer are configured to vary the amount of sag of the initial water layer (6.4 mm thick) caused by its weight. The least amount of sag is configured by using a single layer of mylar film with the support wires. A moderate amount of sag is configured by using five layers of mylar film without support wires. The large sag configuration uses a single layer of mylar film without the support wires. Delay of the peak pressures are clearly seen in Fig 9. The greater the initial sag, the longer the delay of the peak pressure. The total energy of the impact is conserved by a decrease of the peak pressure as the peak is further delayed.

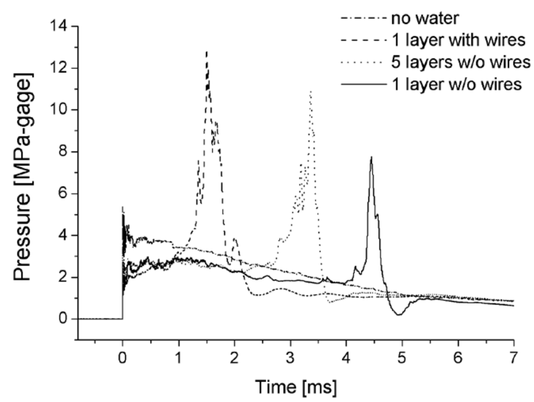

Fig. 9: Comparison of pressure histories at the end-wall ($M = 2.65$) for different initial water layer profiles.

Many shock water layer experiments have been conducted at several Mach numbers ranging from 1.34 to 3.20, and the peak pressures at the end-wall are plotted as a function of the incident shock wave Mach number in Fig. 10. The peak pressures calculated from the theoretical model are plotted as maximum possible peak pressure. As observed in the pressure traces: 1) a thicker water layer results in a higher peak pressure, 2) a stronger incident shock wave results in a higher peak pressure, and 3) the experimental peak pressures are always less than that from the piston model as expected.

In 1973, Nuckolls et al.[12] stated that a fusion microexplosion produces no more impulsive force than a large firecracker since the debris mass is very small. This statement may not be true for the thick-liquid protection reactor design since a pocket of molten FLiBe that surrounds the fusion target will absorb most of the energy from the fusion reaction and this accelerated molten salt will be part of the explosion debris mass which is many times heavier than the fusion debris itself. However, in a spherical geometry, as is the case in most IFE reactor designs, the increase in peak pressure due to the liquid wall protection will be less than that in a uniform cross-section shock tube. In the shock tube the wave is confined, but in a reaction

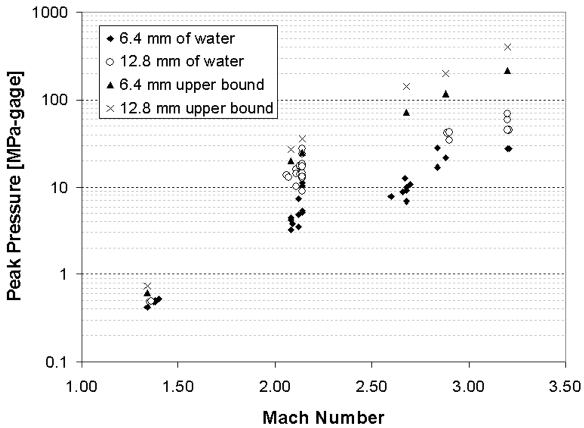

Fig. 10: End-wall peak pressure as a function of incident shock wave Mach number compared to the theoretical model as upper bounds of the experiments.

chamber, both the shock wave and the shocked liquid layer will propagate out spherically. Vent channels of the liquid pocket in a thick-liquid protection design[1, 10] are an important feature to reduce pressure load to the wall.

V. CONCLUSIONS

The initially flat water layer becomes highly unstable when subjected to a shock wave. Speed and strength of the transmitted shock wave are reduced after passing through the liquid layer; however, significantly higher peak pressures are observed in the strong shock experiments ($M > 2.0$) when a thicker water layer is present. The end-wall peak pressure increases as the thickness of the water layer and/or Mach number of the incident shock wave increases. All of the peak pressures from the experiments are smaller than those from the theoretical model calculations since the liquid layer does break up and the process is anisentropic. The initial shape of the water layer has a strong effect on the end-wall pressure trace with the pressure always remaining significantly high. This may present a serious challenge in designing the reactor first wall and cooling tubes.

A cylinder can be placed in the test section to simulate a cooling tube in the reactor wall and the pressure distribution around the cylinder can be studied for the impulsive loading from the water layer in the same setup we have already used to study shock-cylinder interactions[11].

ACKNOWLEDGMENTS

Funding for this work was provided by the U. S. Department of Energy under contract number DE-FG02-97ER54413.

REFERENCES

[1] R. W. MOIR et al., "HYLIFE-II: A molten-salt inertial fusion energy power plant design–final report," *Fusion Technology*, **25**, 5 (1994).

[2] H. MORIYAMA, "Chemical behaviors of tritium formed in a LiF-BeF_2 mixture," *J. of Nuclear Materials*, **148**, 211 (1986).

[3] T. TERAI et al., "Tritium release from Li_2BeF_4 molten salt breeder under neutron irradiation at elevated temperature," *Fusion Technology*, **39 n.2-2**, 768 (2001).

[4] L. C. ELWELL et al., "Dynamics of oscillating turbulent liquid sheets," *Fusion Technology*, **39 n.2-2**, 716 (2001).

[5] R. ABBOTT et al., "Cylindrical liquid jet grids for beam-port protection of thick-liquid heavy-ion fusion target chambers," *Fusion Technology*, **39 n.2-2**, 732 (2001).

[6] S. J. PEMBERTON, *Thick Liquid Protection in Inertial Fusion Power Plants*, Ph.D. thesis, University of California-Berkeley, Berkeley CA (2002).

[7] W. K. CHONG et al., "A comparison of simulation's results with experiment on water mitigation of an explosion," *J. of Shock and Vibration*, **6**, 73 (1999).

[8] H. Z. ZHAO, K. Y. LAM and O. Y. CHONG, "Water mitigation effects on the detonations in confined chamber and tunnel system," *J. of Shock and Vibration*, **8**, 349 (2001).

[9] C. JANTZEN and P. F. PETERSON, "Scaled impulse loading for liquid hydraulic response in IFE thick-liquid chamber experiments," *Nuclear Instrument & Methods in Physics Research*, **A 464**, 404 (2001).

[10] P. F. PETERSON, "Design methods for thick-liquid protection of inertial fusion chambers," *Fusion Technology*, **39 n.2-2**, 702 (2001).

[11] J. OAKLEY et al., "Shock loading of a cylinder bank with imaging a pressure measurements," *The 23rd International Symposium on Shock Waves*, Fort Worth TX (2001).

[12] J. NUCKOLLS, J. EMMETT and L. WOOD, "Laser-induced thermonuclear fusion," *Physics Today*, 46 (August 1973).